

Loads and Stability Analysis of an Unmanned Tilt Rotor

Matthew W. Floros
Aerospace Engineer
Army Research Laboratory
Hampton, Virginia

Jinwei Shen
Aerospace Engineer
National Institute of Aerospace
Hampton, Virginia

Myeong Kyu Lee
Senior Engineer
Korea Aerospace Research Institute
Daejeon, Korea

Soojung Hwang
Senior Researcher

Loads and stability calculations for a proposed unmanned tilt rotor aircraft are presented. Blade loads are calculated using the comprehensive analysis CAMRAD II and the multibody dynamics analysis DYMORE II for helicopter, airplane, transition, and maneuvering flight. Gust loadings are investigated for some of the maneuvers. Good agreement of bending loads is seen between the two analyses, particularly in airplane mode. Torsion moments differ substantially between the two analyses with the smallest difference in airplane mode. Rotor-wing stability is examined using DYMORE II. A parametric study of wing beam mode damping with varying rotor and wing properties for semi-span and full-span models is presented. No instabilities are observed for the parameters examined. Beam mode damping is found to be particularly sensitive to blade precone angle, wing torsion stiffness, and pylon conversion actuator stiffness. Reduced fuselage roll inertia due to fuel burn is found to increase beam mode damping. Correlations of isolated rotor lag frequencies and damping ratios between the two analyses also compare favorably.

Introduction

Recently, there has been increased investment in advanced simulation and modeling for rotorcraft. The high cost of wind tunnel and flight test experiments and the decreased availability of experimental facilities have prompted the use of computational alternatives. Systematic use of these analytical models currently supplements and may eventually supplant experimental verifications. In particular, parameter variations which are expensive or difficult to implement on a physical model can readily be examined in simulation.

Though computational tools are not yet approaching the fidelity required to replace wind tunnel or flight tests, in the design phase, before hardware is fabricated, comprehensive analysis and simulation are the only tools available to guide and assess the proposed design. Even if test data are available, simulation tools can be employed to explain unexpected results or provide valuable insight into the physics behind test data. A large array of analytical sensors not possible on a physical model can be deployed in simulation to provide fine details for the researcher.

Comprehensive, multibody-based analyses of rotorcraft enable the modeling and simulation of the rotor system to a high level of detail such that complex mechanics and nonlinear effects associated with the control system geometry and pylon conversion assembly can be considered. Kinematics of hub components can have a strong effect on the stability of the rotor system.

In this paper, a rotor and wing for a proposed tilt-rotor aircraft are examined using the comprehensive analysis CAMRAD II (Ref. 1) and the multibody dynamics analysis DYMORE II (Ref. 2). Both analyses have been applied to the analysis of tilt rotors in the past (Refs. 3, 4). The data presented in the paper are the result of calculations performed in support of the vehicle design. Some limited results were previously reported by Shen, Floros, *et al* (Ref. 5). A rendering of the aircraft is shown in Figure 1 and vehicle properties are given in Table 1.

The analytical models were developed in parallel so that the geometry, mass, and stiffness properties of the rotor match. Although some different modeling choices were made, the two models were intended to match as closely as possible. Initially, concurrent loads and stability calculations from both analyses were planned. Because of time and budget constraints, the effort was divided such that the loads calculations were performed with CAMRAD II and most of the stability

Report Documentation Page

*Form Approved
OMB No. 0704-0188*

Public reporting burden for the collection of information is estimated to average 1 hour per response, including the time for reviewing instructions, searching existing data sources, gathering and maintaining the data needed, and completing and reviewing the collection of information. Send comments regarding this burden estimate or any other aspect of this collection of information, including suggestions for reducing this burden, to Washington Headquarters Services, Directorate for Information Operations and Reports, 1215 Jefferson Davis Highway, Suite 1204, Arlington VA 22202-4302. Respondents should be aware that notwithstanding any other provision of law, no person shall be subject to a penalty for failing to comply with a collection of information if it does not display a currently valid OMB control number.

1. REPORT DATE MAY 2006	2. REPORT TYPE	3. DATES COVERED 00-00-2006 to 00-00-2006			
4. TITLE AND SUBTITLE Loads and Stability Analysis of an Unmanned Tilt Rotor		5a. CONTRACT NUMBER			
		5b. GRANT NUMBER			
		5c. PROGRAM ELEMENT NUMBER			
6. AUTHOR(S)		5d. PROJECT NUMBER			
		5e. TASK NUMBER			
		5f. WORK UNIT NUMBER			
7. PERFORMING ORGANIZATION NAME(S) AND ADDRESS(ES) Army Research Laboratory, Hampton, VA, 23681		8. PERFORMING ORGANIZATION REPORT NUMBER			
9. SPONSORING/MONITORING AGENCY NAME(S) AND ADDRESS(ES)		10. SPONSOR/MONITOR'S ACRONYM(S)			
		11. SPONSOR/MONITOR'S REPORT NUMBER(S)			
12. DISTRIBUTION/AVAILABILITY STATEMENT Approved for public release; distribution unlimited					
13. SUPPLEMENTARY NOTES					
14. ABSTRACT					
15. SUBJECT TERMS					
16. SECURITY CLASSIFICATION OF:			17. LIMITATION OF ABSTRACT Same as Report (SAR)	18. NUMBER OF PAGES 19	19a. NAME OF RESPONSIBLE PERSON
a. REPORT unclassified	b. ABSTRACT unclassified	c. THIS PAGE unclassified			

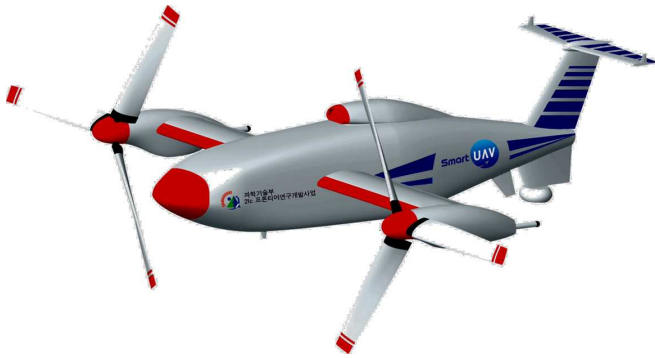


Fig. 1. Artist rendering of proposed tilt rotor aircraft.

Table 1. Tilt rotor aircraft physical properties.

Gross Weight	2000 lb
Maximum Speed	270 kts
Wingspan	22.3 ft
Fuselage Length	16.4 ft
Rotor Configuration	Gimbal
Number of Blades	3
Rotor Diameter	9.4 ft
Airplane Rotor Speed	1284 RPM
Helicopter Rotor Speed	1605 RPM

calculations were performed using DYMORE with only a few stability calculations in CAMRAD II. However, some loads and stability cases were compared between the analyses to verify that they produce consistent results.

Analytical Models

The rotor being analyzed is a 3-bladed, stiff inplane, gimbaled rotor. A schematic of the hub is shown in Figure 2. Each blade is connected to the hub through a flexure which is softer in bending than the surrounding structure. Pitch control is provided by a torque tube surrounding the flexure and a feathering spindle. Inside the feathering spindle is a tension-torsion strap designed to carry the large axial loads from centrifugal forces, but be soft in both bending and torsion.

The CAMRAD II model used in the loads analysis was an isolated rotor model, while elastic semi- and full-span models were developed for stability analysis in DYMORE II. Where the wing and pylon dimensions were needed, a rigid wing was added to the CAMRAD II model. The rotor models, while not identical, were developed from the same drawings and property data. Modal reduction was used for the blades in CAMRAD II, where the entire DYMORE II model was used in the analysis. The CAMRAD II and DYMORE II models are shown in Figures 3 and 4, respectively.

A common modeling assumption in comprehensive rotor analyses is that the blades are identical so only one blade must

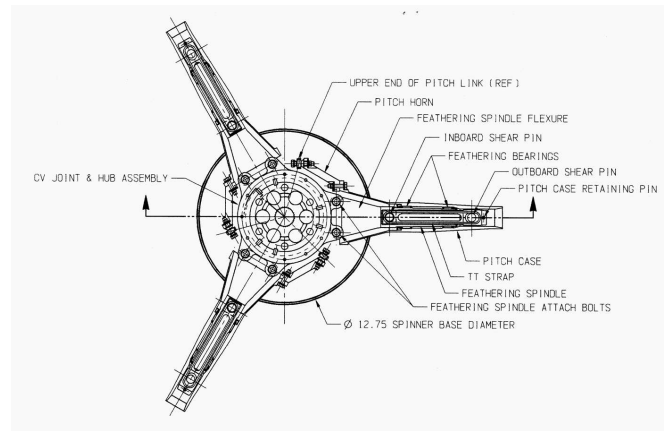


Fig. 2. Schematic of three-blade gimbaled hub.

be analyzed and the response and loads of the others are assumed to be the same. A gimbaled rotor system couples the three blades through the gimbal, so such an assumption is not valid. Rather, the response of the three blades together must be considered. The blades were modeled as elastic beams joined together at the hub. The hub was considered rigid, with joints for the rotation and gimbal motion.

A recurring challenge in comprehensive analysis is the choice of the appropriate level of analysis detail. Modern multibody dynamics-based analyses allow for detailed swashplate models that are increasingly common in rotor analyses. For the current work, the swashplate control system was modeled. The pitch horns and the swashplate itself were modeled as rigid bodies, and the flexibility of the control system was accounted for with pitch link axial stiffness.

In reality, the majority of control system compliance is often found in pitch horn bending, and axial deformation of the pitch link is relatively small. While this distinction may be important for the blade and hub designer, it is not typically relevant for calculation of blade loads. There is sometimes the tendency to over-model fine linkages and parts because the analysis has the ability to do so. Such an approach can lead to a very complex model with little improvement in accuracy. A pitch horn, for example is often short and stubby and would not be appropriately modeled with the beam elements available in either CAMRAD II or DYMORE. In the current work, the control system compliance was calculated with a detailed finite element model and lumped together as pitch link stiffness for the rotorcraft analyses. This is a common practice.

One improvement multibody dynamics-based analysis provides over traditional rotorcraft analyses is the capability for dual load paths. The most common example is the pitch link providing a second load path to the blade. Additional load paths can be modeled in the case of multiple structure designs, such as strap packs.

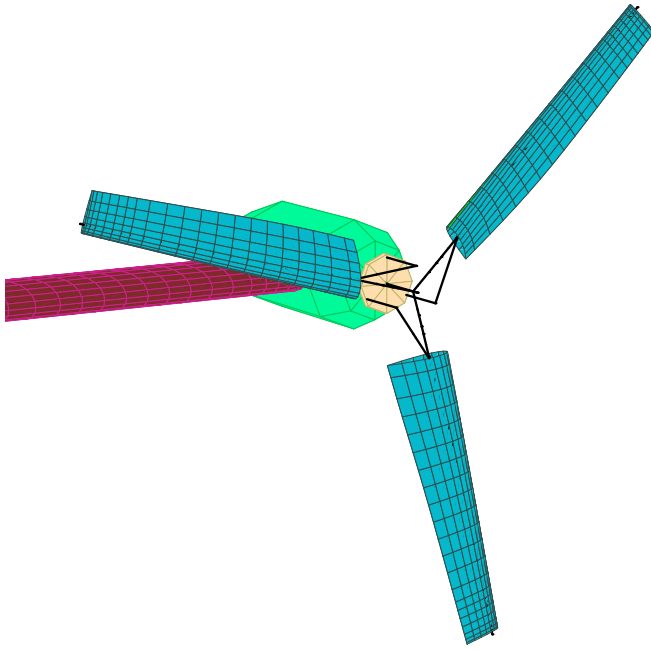


Fig. 3. CAMRAD II rotor model shown with rigid wing and pylon.

In the current work, two load paths to the blade are modeled, the primary load path through the flexure, and the path through the pitch horn. The blade root as designed, shown in Figure 2, had multiple load paths in addition to the pitch control. These are within the blade root itself and include the pitch case, feathering spindle, and tension-torsion strap to react torsion, bending, and axial loads, respectively. These three concentric structures are connected together at the outboard end of the pitch spindle.

It is possible to consider the separate structures, but the model is only improved if the properties of each structure are known accurately and the individual motions of the parts have a measurable effect on the system. Otherwise, the complexity of the model is increased to no benefit. In both models the concentric parts were combined into a single beam with a discrete pitch bearing. In the CAMRAD II model, the pitch bearing was located at the outer end of the pitch spindle, while in the DYMORE II model it was in the center of the spindle. The axial stiffness of the tension-torsion strap, the bending stiffness of the pitch spindle, and the torsion stiffness of the torque tube were incorporated into the single structure. This assumption is valid to the extent each structure is stiff with respect to the load it is intended to react and soft compared to the others. A pitch bearing spring was also included to model the small torsion stiffness of the tension-torsion strap.

The outer blade was modeled as an elastic beam with appropriate distributed mass and stiffness properties. Additional discrete masses were also introduced at the root of each blade to account for the mass and inertia of the hub and gimbal. A

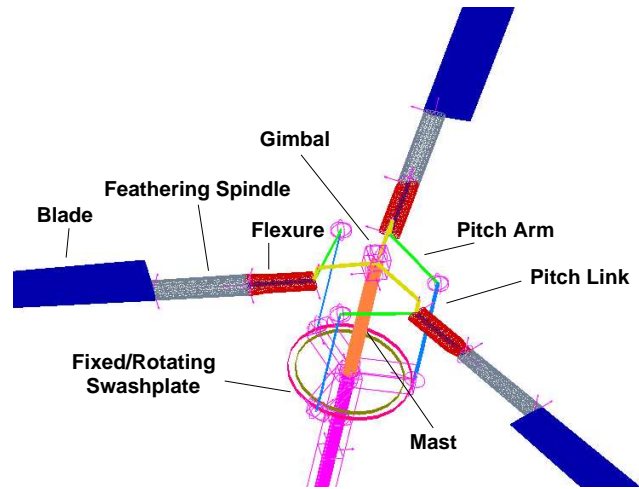


Fig. 4. DYMORE II rotor model.

tip mass for each blade was accounted for in the distributed properties. Other rotor parts, such as the swashplate and pitch horn were modeled as rigid.

A consequence of using multibody dynamics analyses is that traditional quantities used by engineers and scientists are not as straightforward as in traditional rotorcraft analyses. In particular, collective pitch was traditionally straightforward. In a multibody dynamics analysis with a swashplate model, collective pitch is adjusted by linear translation of the swashplate. For a helicopter, a linear relationship between swashplate translation and blade collective pitch angle can be established. For a tilt rotor, however, where the collective pitch travel is on the order of sixty degrees, the relationship between the swashplate motion and the pitch bearing rotation is not necessarily linear. This is especially true in high speed airplane mode flight, where the swashplate is near the end of its travel. For this reason, the term *collective pitch* used in this paper is interchangeable with *collective setting* and represents a linearized quantity related to swashplate motion. It is close to, but not exactly the same as the collective rotations of the pitch bearings.

For the DYMORE II model, the rotor was attached to a fixed wing to form a semi-span model. A full span model, with a mirrored second rotor and full-span wing, was also developed. The pylon conversion actuator was modeled as a flexible joint, which consists of a set of concentrated springs and dampers.

Although often applied to the same problems, CAMRAD II and DYMORE II are very different analyses in their history, formulation, and solution procedures. CAMRAD II provides both harmonic analysis and time integration of equations of motion, where DYMORE II is a strictly time domain analysis. Both analyses, however, are more mathematically rigorous than classical analyses and each has its strengths and weaknesses that can make one more suitable than the other

Table 2. Qualitative descriptions of blade loads cases.

Helicopter Mode		
	Steady	Gust
Max Speed, 80 deg Nacelle	X	
Max Speed, 90 deg Nacelle	X	
Hover, Max Gross	X	X
Vertical Ascent, Max Gross	X	X
Vertical Ascent, Min Gross	X	X
Transition		
	Steady	Gust
Normal Conversion Corridor	X	
Upper Conversion Corridor	X	X
Airplane Mode		
	Steady	Gust
Maximum Speed	X	X
Cruise Speed	X	
Loiter Speed	X	
Maneuvers		
	Steady	Gust
Symmetric Pull-up	X	X
Rolling Pull-up	X	X

for a particular problem. Both are readily applied to loads and stability analysis.

Loads Analysis

The loads cases examined in the current work were provided by the Korea Aerospace Research Institute (KARI), the makers of the aircraft. They represent a sampling of both normal and peak loads the rotor should experience during operation. Load cases for helicopter mode, transition, and airplane mode were analyzed. Blade loads were calculated for steady state and maneuvering flight in smooth air and with gusts. A summary of the cases is given in Table 2.

Early in the design process, loads were calculated with both CAMRAD II and DYMORE II for comparison. As the design progressed and changes were made to dimensions and elastic properties of the vehicle, the stability and loads tasks were divided. While the loads for the final design are most valuable to the vehicle designers and structural engineers, they are not necessarily of general academic interest. The early loads calculations, however, represent a comparison of models developed from the same starting information by two different analysts using two different analyses.

Taking into consideration radial distribution of loading, the cases listed in Table 2 represent a large amount of potential loads data not readily distilled into a few plots. So only a small sampling of illustrative results are presented in this paper. The critical cases for loads were found to be transition between airplane and helicopter modes and the transient maneuvers.

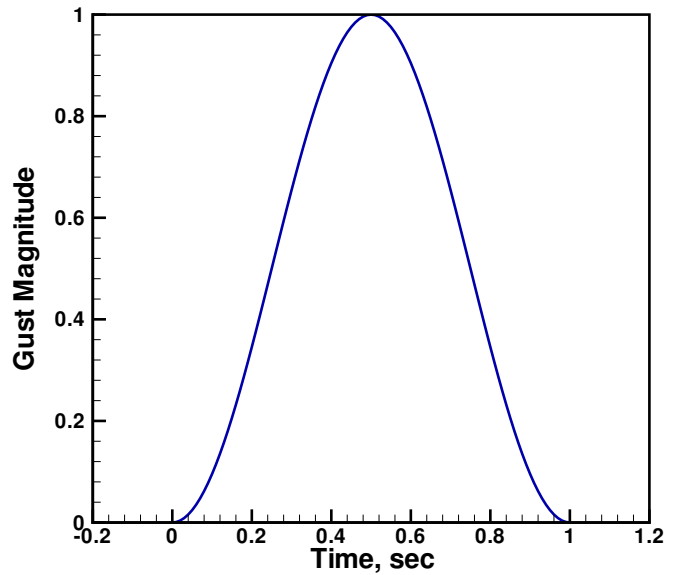


Fig. 5. Non-dimensional gust profile used in loads calculations.

These as well as representative forward flight cases in both airplane mode and helicopter mode are presented.

For steady state loads, CAMRAD II calculates periodic response using a harmonic balance method. An iterative procedure is used to calculate trim settings. In DYMORE, an autopilot feature is used to reach a steady-state trim solution as the equations are integrated in time.

DYMORE has no assumptions about periodic motion, so gusts can be directly applied in DYMORE in its normal operation. In addition to the periodic response and trim task, CAMRAD II features a separate transient analysis task that time integrates the equations of motion similar to DYMORE. For the gust cases, where the rotor motion is not periodic, this transient task must be used in CAMRAD II. The gust profile is shown in Figure 5. For all of the load cases involving gusts, the gust had a 1-second duration, although the magnitude of the gust was different depending on flight condition.

CAMRAD II has several options for calculating blade loads. For the current study, loads were calculated with the default method, based on force summation. Internal and external forces are integrated along the span to produce blade loads. Conversely, DYMORE II calculates blade loads using a curvature method, where the blade displacements are calculated from the blade deflections and stiffness properties.

Helicopter Mode

The first test case is high speed forward flight in helicopter mode. To obtain the flight condition, the airspeed was fixed to 92 kts and the rotor was trimmed to a specified thrust and flapping. Trimming to thrust circumvents the issue of collective

pitch vs. collective pitch bearing rotation described above. The shaft angle was set near 90 deg to incorporate both a 90 deg nacelle angle plus a correction for the vehicle attitude.

The mean and half peak-to-peak blade loads are shown in Figure 6. The correlation in the mean bending loads is quite good. The flap bending moments, shown in Figure 6a, match very closely except for the midspan, where CAMRAD II predicts a larger positive moment than DYMORE II. The mean lagwise bending loads (Figure 6b), also match very closely except for approximately 30% radius, where again CAMRAD II predicts a larger moment. The half peak-to-peak bending loads, shown in Figure 6d and e, are very close over the entire span.

The torsion moments, shown in Figure 6c and 6f, do not match as well. There is approximately a factor of two difference in the mean moment and a factor of three in the oscillatory moment. The shape of the curves is very similar, however. Note that the pitch bearing was placed at 18% radius in the CAMRAD II model and approximately 14% in the DYMORE II model. These correspond to the outboard end and center of the pitch spindle (see Figure 2). That is the reason for the step changes in the torsion moment at those radial stations in the plots. The loads are calculated in the blade principal axes, not the hub plane. In many of the results, there are step changes in bending and torsion moments because of the pitch bearing.

Airplane Mode

Two cases are presented for airplane mode flight, a cruise condition, 216 kts, and a high speed flight condition, 270 kts. The cruise condition is the initial condition for the transient maneuvers described below. Like the helicopter mode calculations, the airspeed was specified and the rotor was trimmed to specified thrust and flapping. Trimming to thrust is especially important in airplane mode, where there is a large amount of axial flow and the rotor is lightly loaded. Very small increments in collective pitch have a dramatic effect on rotor thrust.

Loads in cruise flight are shown in Figure 7. The mean loads compare well for both flap and lag bending, Figure 7a and b. The mean torsion moments (Figure 7c) do not agree as well as the flap and lag bending moments, but the predictions differ by approximately 50% rather than 100% as seen in Figure 6c. The nearly axisymmetric loading resulted in the best correlation for torsion moments in the study to be exhibited in the airplane mode cases.

The oscillatory flap and lag bending loads do not match as closely as the mean loads, but nonetheless agree well. The half peak-to-peak flap moments (Figure 7d) have a similar trend except for what appears to be a radial offset between 0.4R and 0.8R. It is not clear what might cause moments to differ radially between the two analyses. The moderately sloped lines can be brought together by either horizontal or

vertical shift, so what appears to be a radial shift may instead be a magnitude discrepancy.

The DYMORE II-predicted moment is larger at 90% than the CAMRAD II prediction at 80% and remains larger inboard until 0.4R. This might be an artifact of the curvature method for calculating loads. From 0.2R–0.4R, there is a significant deviation between the two predictions, where the CAMRAD II prediction is significantly larger than that from DYMORE II. Inboard of 0.2R the predictions come together again. The lag bending moments in Figure 7e agree well over the entire radius. Finally, the torsion moments (Figure 7f) are small in magnitude, only 1–2 ft-lb, but agree very well inboard of 0.5R and reasonably well outboard.

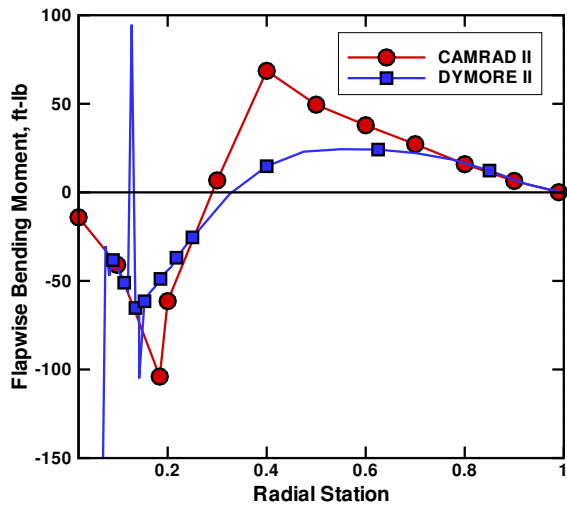
Loads were also calculated in airplane mode at the maximum speed of 270 kts. For the maximum speed case, the loads were calculated in smooth air and with a 50 ft/sec vertical gust. For the gust, a 2.5 second record was simulated with the gust occurring between 1 and 2 seconds. The half peak-to-peak loads are calculated from the extremes of the entire 2.5-second record.

The bending and torsion loads are shown in Figure 8. The rotor was trimmed to specific flapping angles that were small, but not zero. So there are nonzero oscillatory loads in the smooth air case, but they are dwarfed by the half peak-to-peak loads with the gust. The mean and oscillatory bending loads in both flap and lag practically lie on top of each other except for the difference in the radial location of the pitch bearing. The torsion moments with the gust differ by approximately 30% at most and show the same characteristic trend as the previous results.

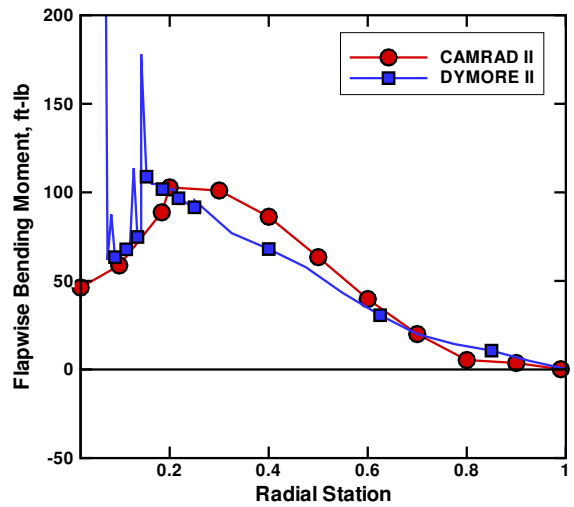
Transition Flight

Transition flight was modeled in steady state. A schedule of nacelle angle, airspeed, thrust, and flapping was provided where each load case was a combination of airspeed and nacelle angle. The CAMRAD II analysis was configured to trim the rotor to the specified thrust and flapping. For the upper conversion corridor, a 30 ft/sec gust loading was also specified. A gust of the same profile was applied from 1–2 seconds of a 2.5-second interval like the airplane mode calculations. Only the magnitude was different.

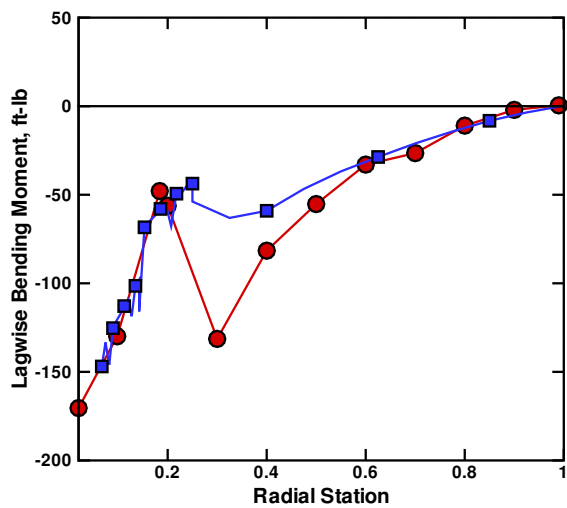
The largest loads were observed for nacelle angles in the 60–75 deg range. Loads for the 60 deg nacelle angle are shown in Figure 9. The forward speed is 121 kts. For a 60 deg nacelle angle, the rotor is between an edgewise condition and an axisymmetric condition. For all of the bending moment calculations, CAMRAD II predicts larger moments than DYMORE II. The mean lagwise moments, Figure 9b, agree better than the flapwise moments, Figure 9a. For both analyses, the gust produces little change in the mean loads. The oscillatory moments in both flap and lag (Figure 9d and e) show similar radial trends but differ in magnitude by 50% to



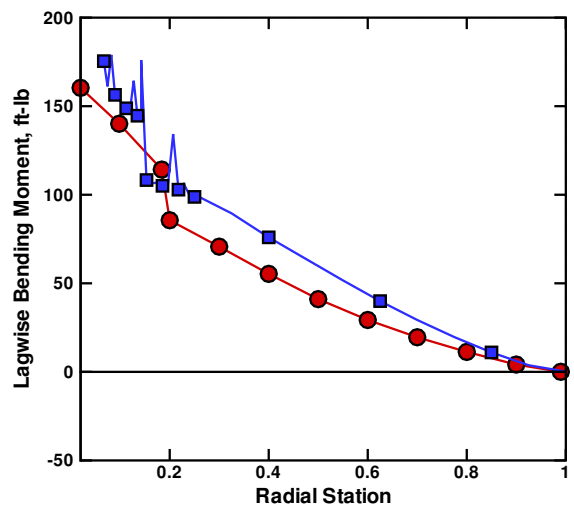
(a) Mean Flap Bending Moment



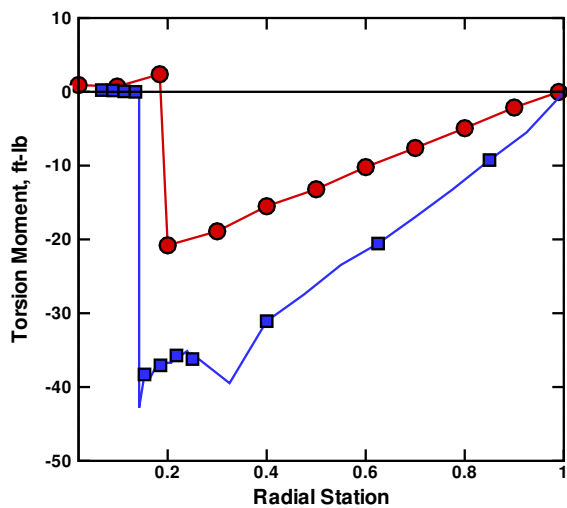
(d) Half Peak-To-Peak Flap Bending Moment



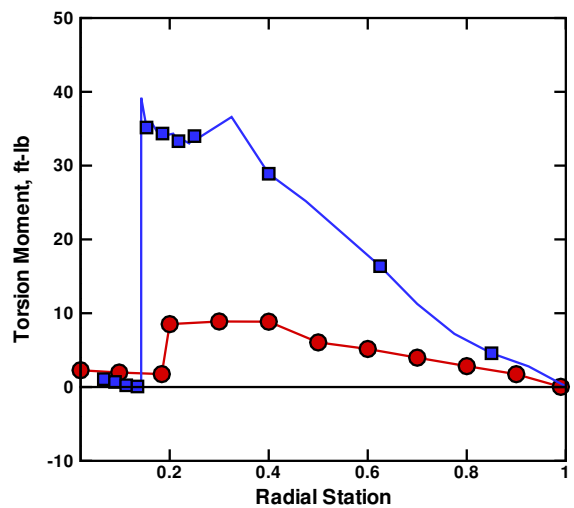
(b) Mean Lag Bending Moment



(e) Half Peak-to-Peak Lag Bending Moment

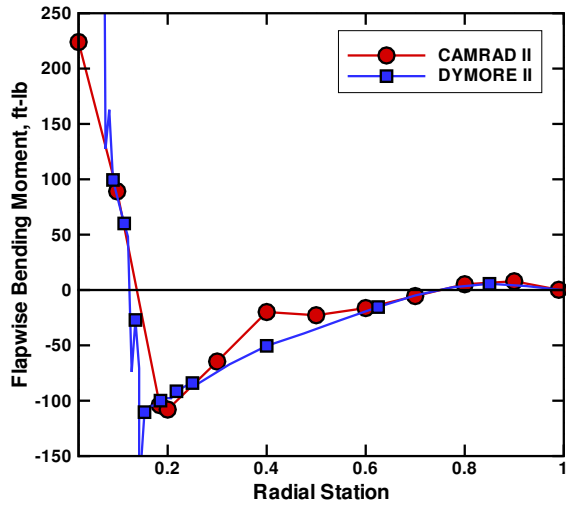


(c) Mean Torsion Moment

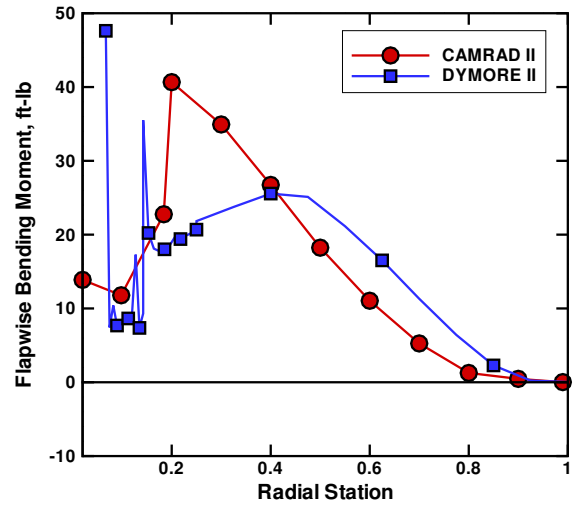


(f) Half Peak-To-Peak Torsion Moment

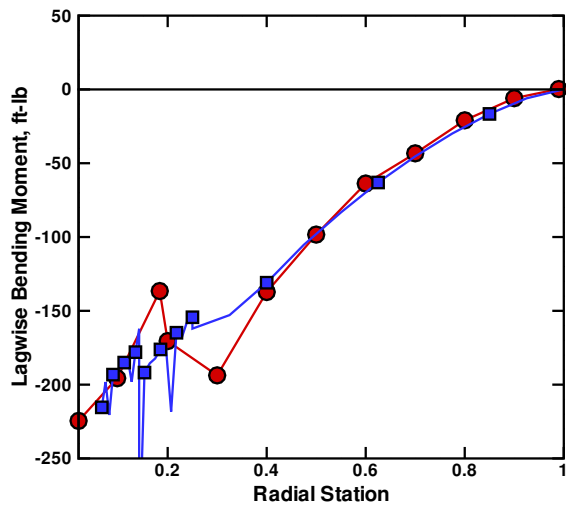
Fig. 6. Comparison of blade loads in helicopter mode, 92 kts airspeed, 90 deg nacelle angle, 1605 RPM.



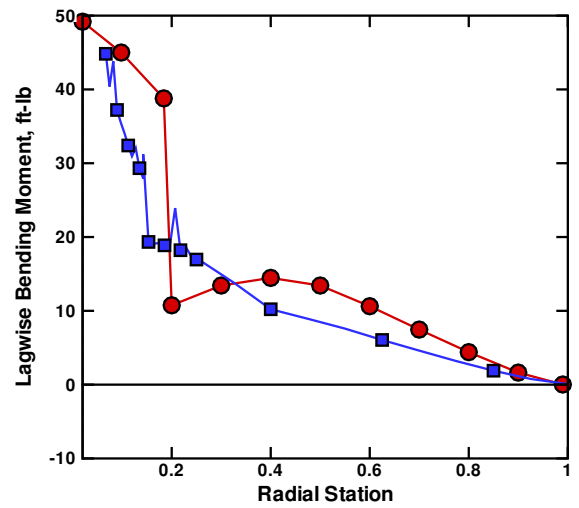
(a) Mean Flap Bending Moment



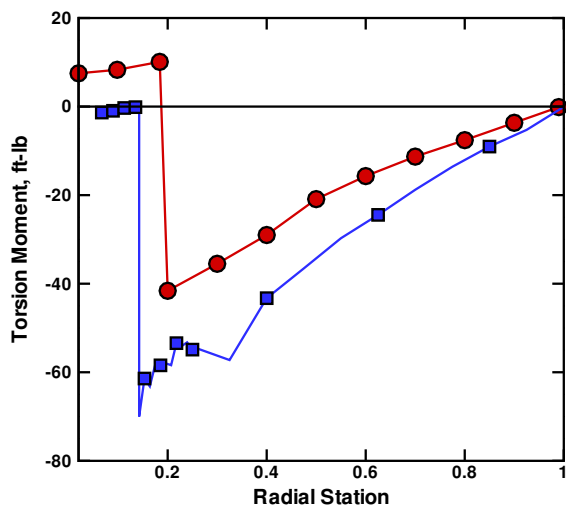
(d) Half Peak-To-Peak Flap Bending Moment



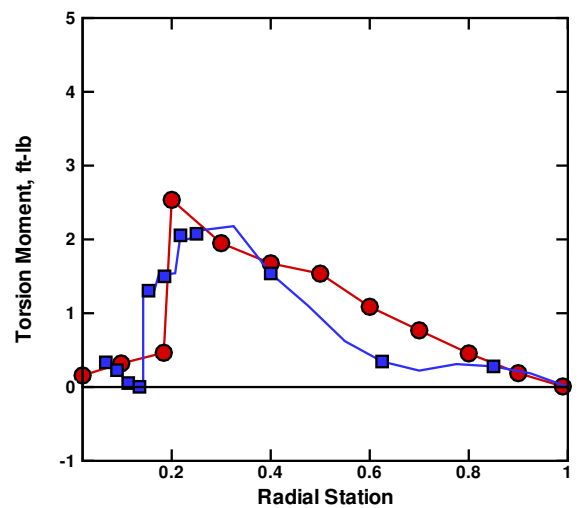
(b) Mean Lag Bending Moment



(e) Half Peak-to-Peak Lag Bending Moment

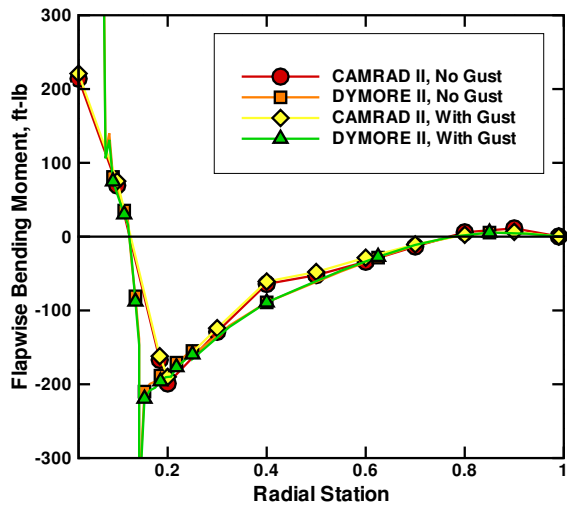


(c) Mean Torsion Moment

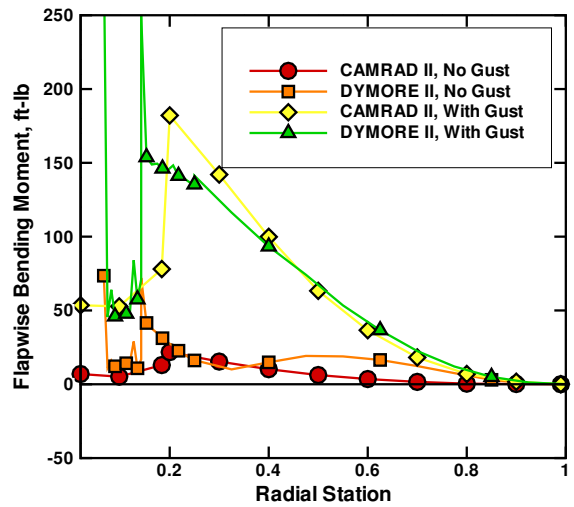


(f) Half Peak-To-Peak Torsion Moment

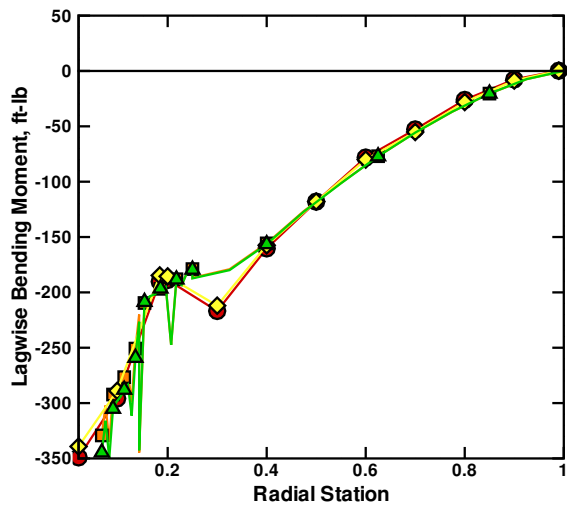
Fig. 7. Comparison of blade loads in airplane mode cruise, 216 kts airspeed, 1284 RPM.



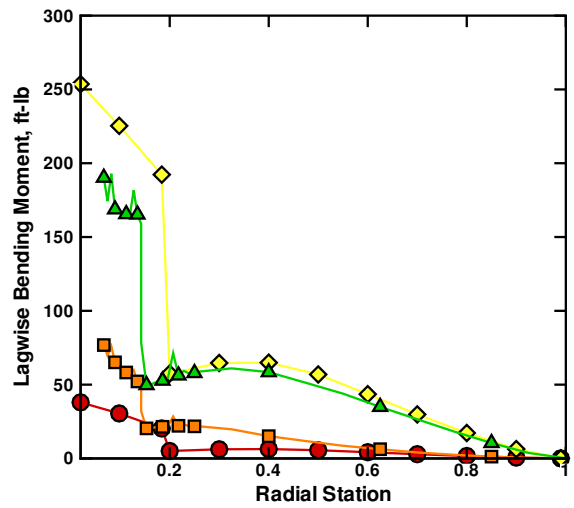
(a) Mean Flap Bending Moment



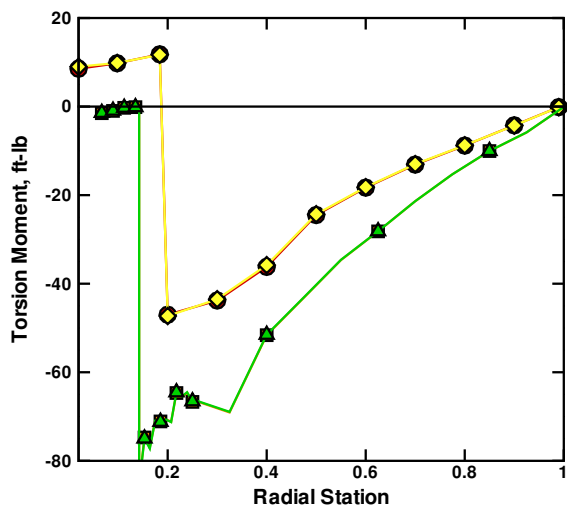
(d) Half Peak-To-Peak Flap Bending Moment



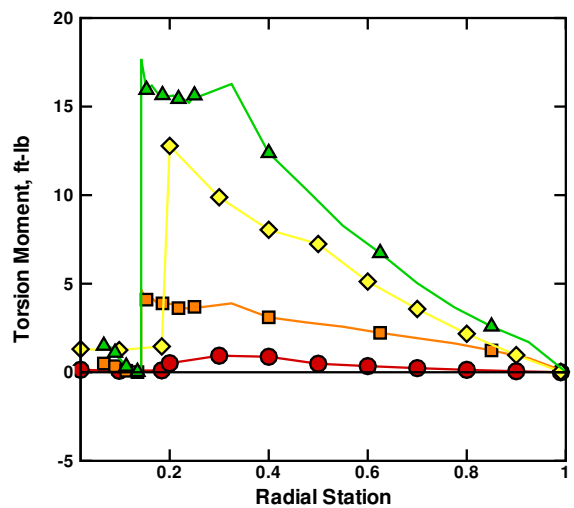
(b) Mean Lag Bending Moment



(e) Half Peak-to-Peak Lag Bending Moment

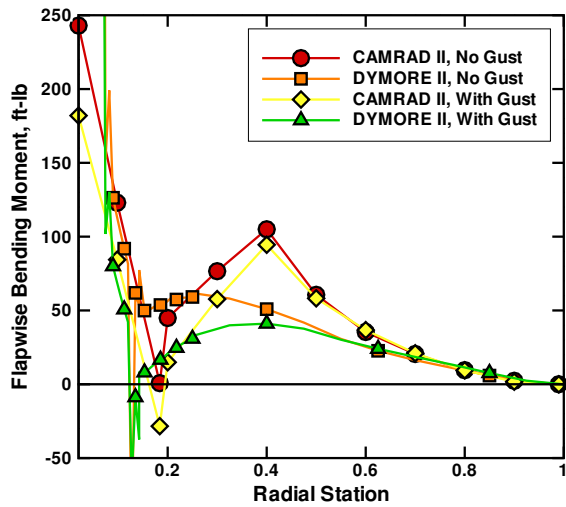


(c) Mean Torsion Moment

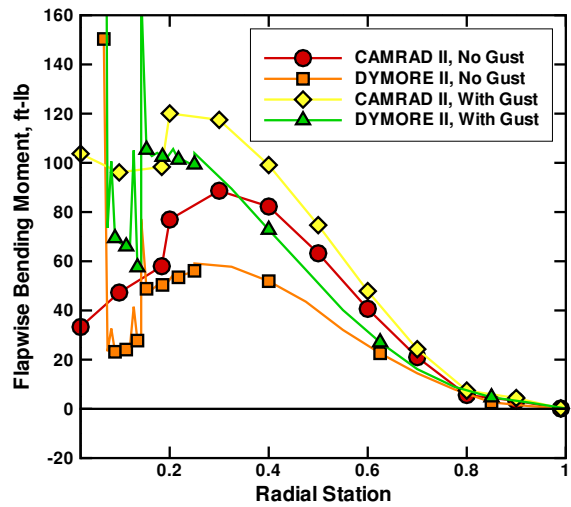


(f) Half Peak-To-Peak Torsion Moment

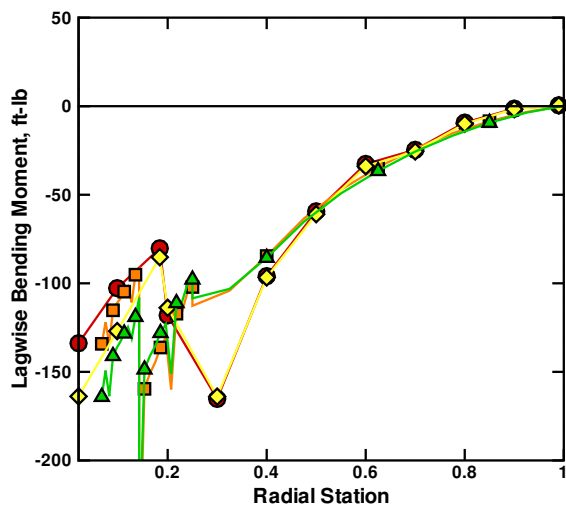
Fig. 8. Comparison of blade loads in high speed airplane mode flight, 270 kts airspeed, 1284 RPM.



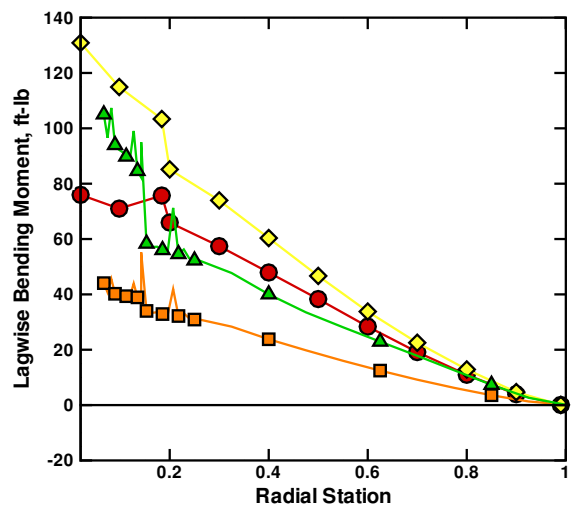
(a) Mean Flap Bending Moment



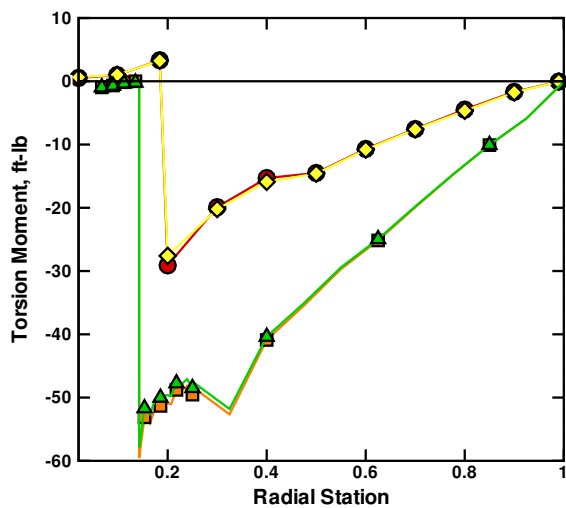
(d) Half Peak-To-Peak Flap Bending Moment



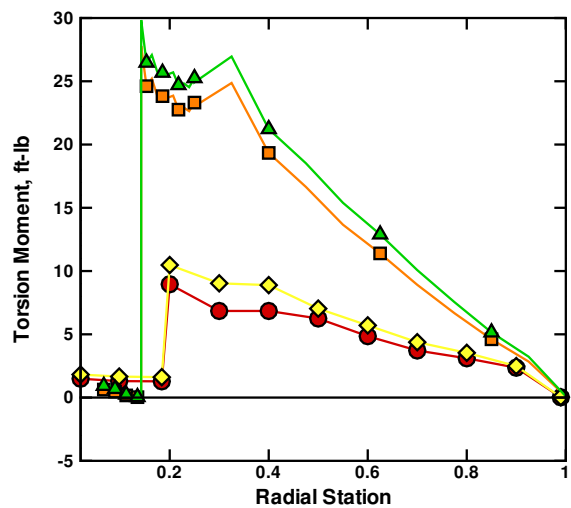
(b) Mean Lag Bending Moment



(e) Half Peak-to-Peak Lag Bending Moment



(c) Mean Torsion Moment



(f) Half Peak-To-Peak Torsion Moment

Fig. 9. Comparison of blade loads in transition flight, 60 deg nacelle angle, 121 kts airspeed, 1605 RPM.

100%. Like the helicopter mode results, both the mean and oscillatory torsion moments differ by a factor of two or three.

Transient Maneuver

The transient maneuvers were analyzed by moving the rotor through a prescribed path. A flight path from an external flight dynamics analysis was supplied, which specified the displacements, velocities, and accelerations of the linear and angular degrees of freedom of the vehicle center of gravity. Blade loads in collision avoidance maneuvers similar to those used in the present study can be found in Reference 6.

For the CAMRAD II analysis, the rotor was attached to a rigid base which was connected to actuators to mimic the flight path. The rotor was offset spanwise and longitudinally from the base on a rigid wing so it was located properly relative to the vehicle c.g. The DYMORE II analysis was configured in a similar fashion.

To ensure consistency between the trim and maneuver conditions in CAMRAD II, the rotor was first trimmed using the same wind tunnel trim procedure as the steady load cases. The velocity of the oncoming wind was set to the forward speed at the start of the maneuver. Rather than suddenly remove the wind and instantaneously start the vehicle motion, the oncoming wind was retained for the duration of the maneuver. The effects of this wind were then subtracted from the vehicle motion. The airspeed schedule was uniformly reduced by the initial airspeed, and the displacement was reduced by the initial airspeed multiplied by time. This provided for a very smooth transition between the trim and transient phases of the analysis.

Only the collective pitch input changed during each maneuver; cyclic pitch was held fixed. The collective pitch followed a predetermined schedule like the vehicle degrees of freedom. The pitch change was also applied as a perturbation. The steady state collective setting specified for trim calculated by the flight dynamics analysis was removed from the collective schedule and the resulting deviation added to the steady state collective determined by CAMRAD II and DYMORE II.

In CAMRAD II, the solution procedures for trim and transient analysis are different, so there is a small discrepancy between the periodic response and the steady state response produced by time integration. The discrepancy must damp out when the transient task is started. Because of the steps taken to ensure compatibility between the trim and transient solutions, the transient task reached steady state within a few rotor revolutions.

Two maneuvers were considered, a symmetric pull-up and a rolling pull-up. Only data from the symmetric pull-up is provided here. For this maneuver, the acceleration is only in the vertical direction, whereas the rolling pull-up has a much more complex flight path. Loads at 40% radius calculated by

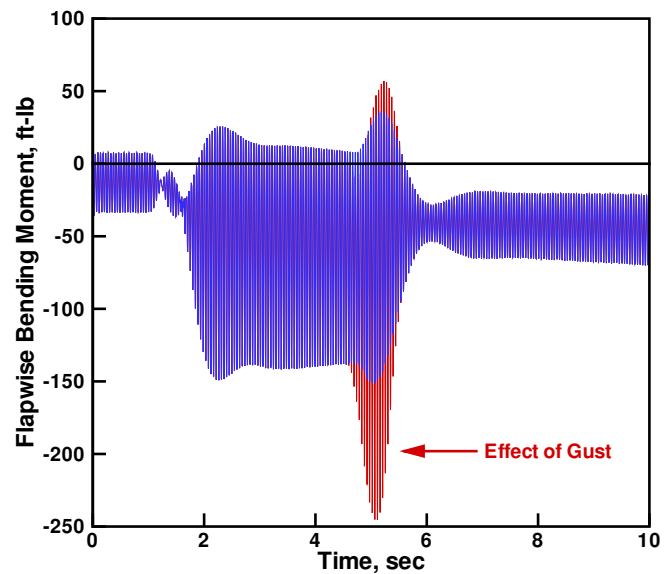


Fig. 10. Time history of CAMRAD II flap bending moments at 0.4R for a symmetric pull-up maneuver in airplane mode with and without gust loading.

CAMRAD II are shown in Figures 10–12. The acceleration portion of the maneuver is from 1–6 seconds, and the vehicle is essentially steady for the remainder of the interval. This is evident in all three plots. The loads are most severe at the beginning and end of the maneuver because of the initial acceleration from steady state and some overshoot beyond the end state. The maneuver as specified does not end in steady level flight. The vehicle is in a steep climb at the end of the maneuver, so the moments at 10 seconds do not and should not match those from 0–1 seconds.

The plots show the magnitude of load that can be produced by a maneuver. The half peak-to-peak flapping loads (Figure 10) in steady state are on the order of 50 ft-lb, but peak at about 200 ft-lb during the maneuver. Lagwise bending and torsion loads (Figures 11 and 12) are also increased significantly over steady state.

The loads cases were run both in smooth air and with the most severe blade loads punctuated by a vertical gust. The loads with the gust, shown in red, are identical to those without the gust except for the interval from 4.5–5.5 seconds where the gust is applied. The gust has the effect of increasing the half peak-to-peak flapping moments by nearly a factor of two and increasing the steady level as well. The effects on lagwise bending and torsion are not so dramatic, but increases on the order of 50% are still observed.

Comparisons of the blade loads calculations from CAMRAD II and DYMORE II are shown in Figure 13. The mean and 1/rev harmonics of flap and lag bending moments are shown with and without the gust loading. The mean and 1/rev sine harmonic of flap bending moments, shown in Figure 13a

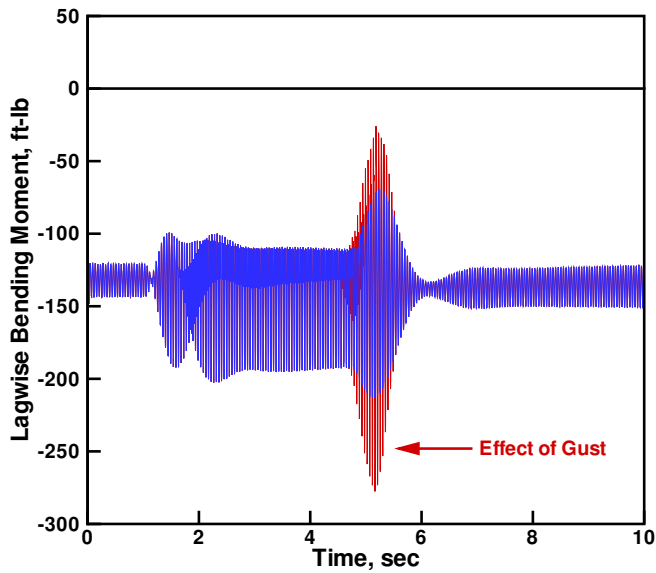


Fig. 11. Time history of CAMRAD II lag bending moments at 0.4R for a symmetric pull-up maneuver in airplane mode with and without gust loading.

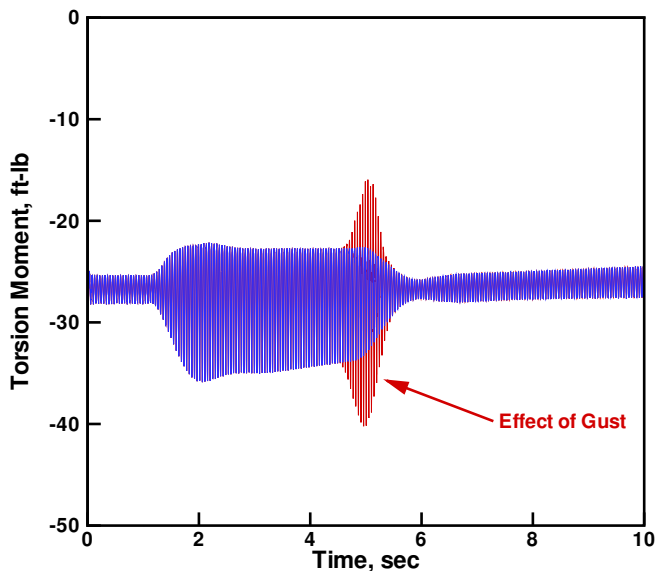


Fig. 12. Time history of CAMRAD II torsion moments at 0.4R for a symmetric pull-up maneuver in airplane mode with and without gust loading.

and b, match very closely between CAMRAD II and DYMORE II. The 1/rev cosine flapping moment correlation (Figure 13c) is good, but the peak moment around 5 seconds into the maneuver differs both with and without the added gust. Overall, however, the three plots demonstrate very good correlation in both magnitude and phase.

The trends for the lag bending moments (Figures 13d–f) are similar. The mean lag moment (Figure 13d) is approximately constant throughout the maneuver, and the addition of the gust does not introduce any substantial deviation. Like the flap bending moments, the 1/rev sine and cosine components agree very well, with the 1/rev sine component showing better agreement than the 1/rev cosine.

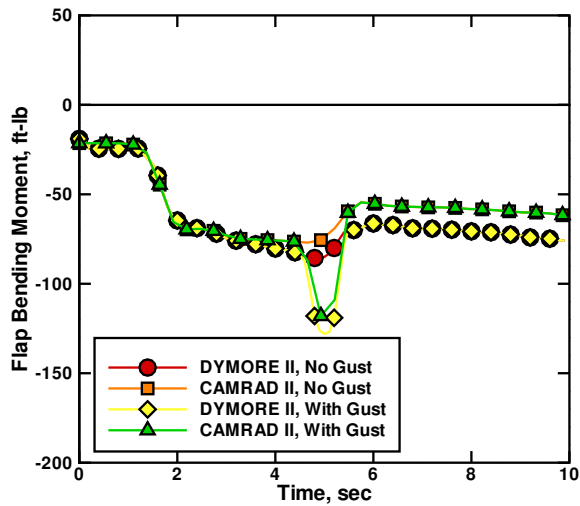
Stability Analysis

The rotor stability was also evaluated using CAMRAD II and DYMORE II. Like loads calculations, the stability calculations are performed differently between the two analyses. Damping was calculated in DYMORE in much the same way as it would be calculated in a wind tunnel test. The rotor was trimmed to a steady-state condition, then the wing was perturbed to produce motion in the mode of interest. For example, to measure damping of the wing beam mode, the wing tip was deflected vertically and released. The free decay of the response was calculated, and damping was calculated from the resulting time history.

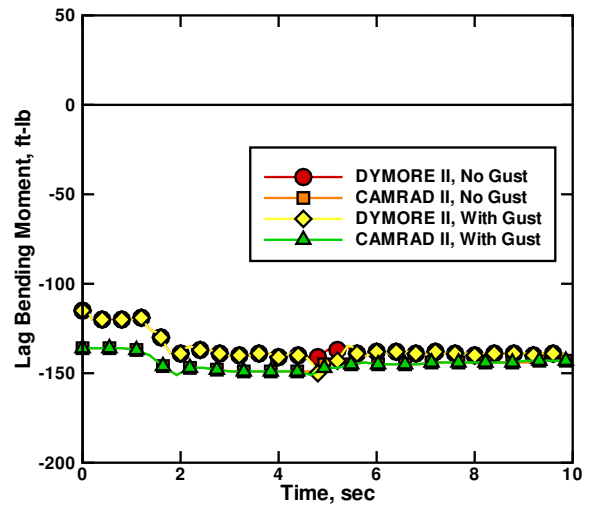
For the DYMORE II results, damping ratios were calculated using Prony’s method, which was shown to be similar to Floquet theory (Ref. 7). An internal comparison between calculations using Prony’s method and the more common moving block method was conducted, and they were found to give the same damping.

Although this “virtual experiment” could be duplicated using CAMRAD II, a different approach was taken to analyze the system stability. In addition to its time integration and harmonic analysis capabilities, CAMRAD II can also calculate linearized eigenvalues. Once a trim condition is reached, the equations are linearized about the trim state and the frequencies and damping are calculated from the system eigenvalues.

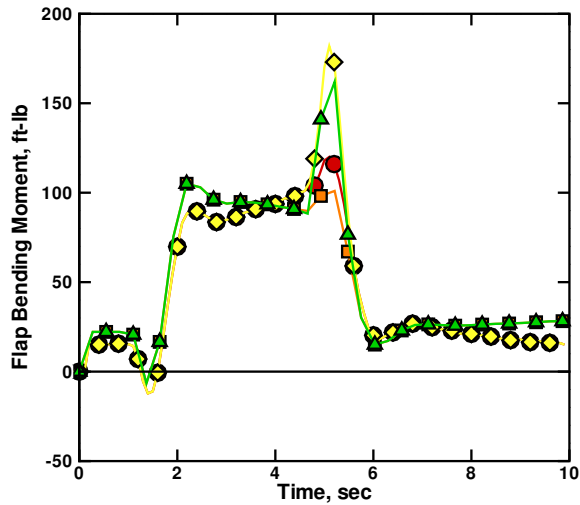
The eigenvalue analysis has the limitation that the results are linearized, and it is sometimes difficult to identify modes. But it has the important benefit of producing the frequency and damping information for a large number of modes simultaneously. The analyst does not need to speculate on what the critical mode might be because damping for all of the modes is provided. Therefore it is a good complement to the DYMORE analysis, where each mode has to be perturbed individually to get a clean damping measurement.



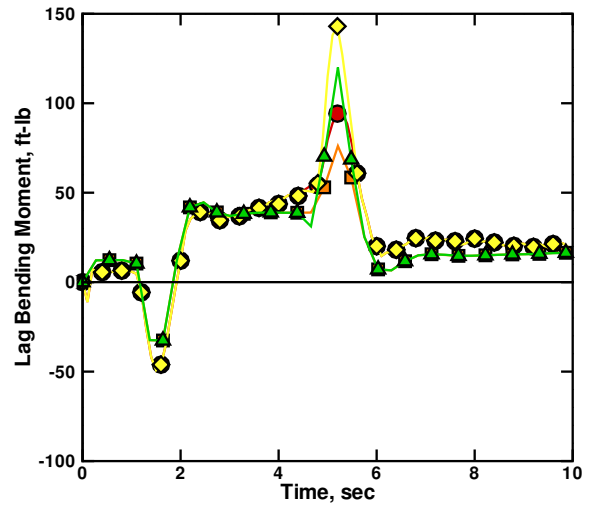
(a) Mean Flap Bending Moment



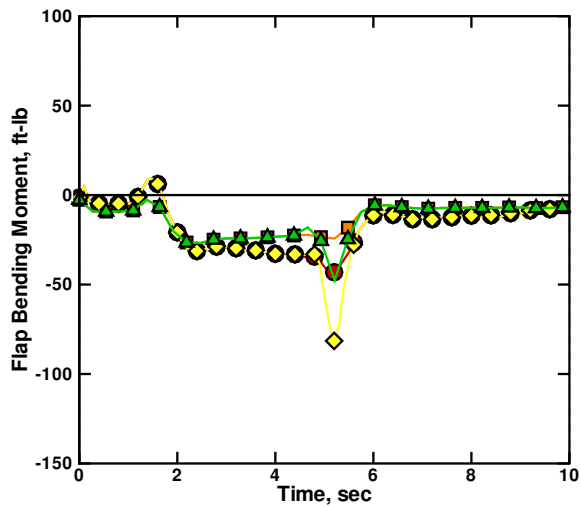
(d) Mean Lag Bending Moment



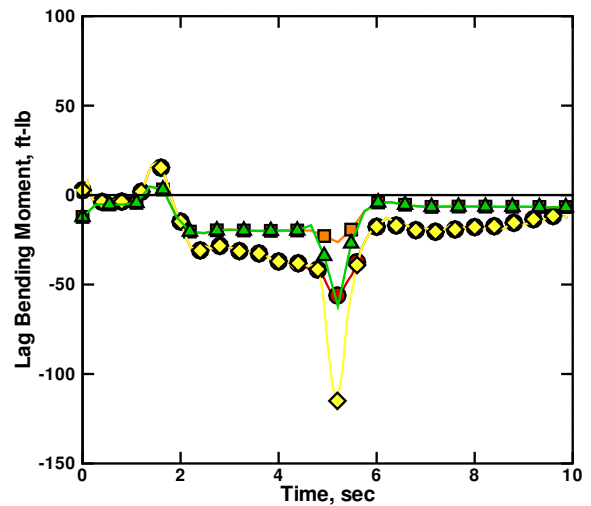
(b) 1/rev Sine Flap Bending Moment



(e) 1/rev Sine Lag Bending Moment



(c) 1/rev Cosine Flap Bending Moment



(f) 1/rev Cosine Lag Bending Moment

Fig. 13. Comparison of blade load harmonics at 0.4R from CAMRAD II and DYMORE II during symmetric pull-up maneuver, airplane mode, 1284 RPM.

Isolated Rotor Stability

Most of the stability analysis was conducted using DYMORE II, but some calculations were made using CAMRAD II. In order to increase confidence that both analyses would give the same answer, some isolated rotor stability calculations were compared between the two analyses. CAMRAD II was not used for any rotor-wing stability calculations, so the analyses could only be compared using isolated rotor models. Note that, like loads calculations, getting the *same* answer from both analyses does not necessarily imply the *correct* answer, but does give confidence in the similarity of the models. The inputs may not represent all of the critical physics of the as-built rotor system, but at least the consistency of the inputs can be determined.

Frequencies and damping ratios over a range of velocities in airplane mode were calculated with both analyses. The lowest damped mode was the lag mode, so only that mode was compared to reduce the number of cases to be run in DYMORE II. As stated earlier, CAMRAD II produces a list of frequencies and damping ratios, but modes must be identified using other information, such as isolated blade frequencies. For the DYMORE calculations, a specific mode is perturbed, so the perturbed mode should dominate the resulting time history. Therefore, the modes for the comparison were identified in DYMORE II by animating the time history.

The frequency and damping results are shown in Figures 14 and 15. CAMRAD II produces three discrete frequencies for each mode, a collective frequency and two cyclic frequencies. In DYMORE II, the cyclic frequencies are identical. Figure 14 shows that both the collective and cyclic frequencies predicted by CAMRAD II are approximately 1 Hz higher than those predicted by DYMORE II. Aside from that, the frequency trends match very closely.

Damping, shown in Figure 15, also matched very closely. The cyclic mode damping calculated from DYMORE is bounded by the two cyclic modes from CAMRAD II, and the trend is similar. The damping ratio of the critical mode, collective lag, is only different by approximately 0.1% between the two analyses, but that 0.1% spans the stability boundary at low speed. CAMRAD II predicts slight negative damping below 150 kts while DYMORE II predicts a slight positive damping to 115 kts.

The calculations do not include structural damping, so the results do not indicate neutral stability at low speed. They indicate that the actual damping is approximately equal to the structural damping. Structural damping can be significant depending on construction. For a composite blade, modal structural damping is typically assumed to be 1–2% plus additional damping in the bearings, joints, and fasteners that is difficult to quantify analytically. Based on these results, the CAMRAD II and DYMORE II models produce very similar frequency and damping results despite the different methods of calculation.

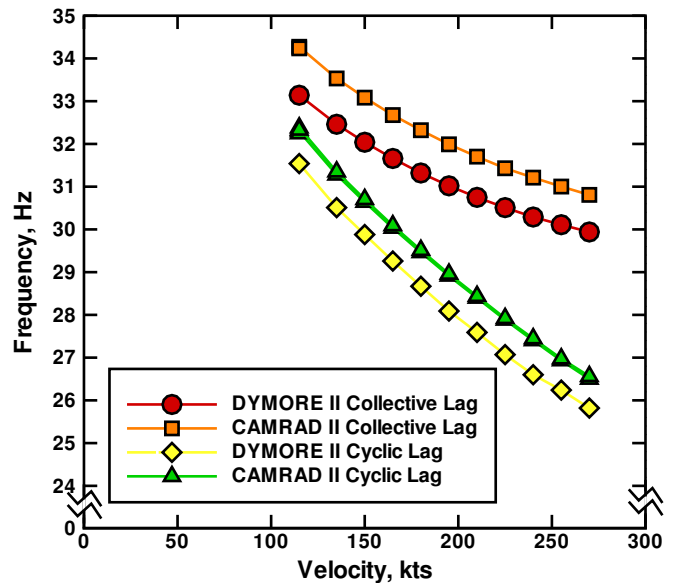


Fig. 14. Comparison of isolated rotor lag bending frequencies from CAMRAD II and DYMORE II calculations, airplane mode, 1284 RPM.

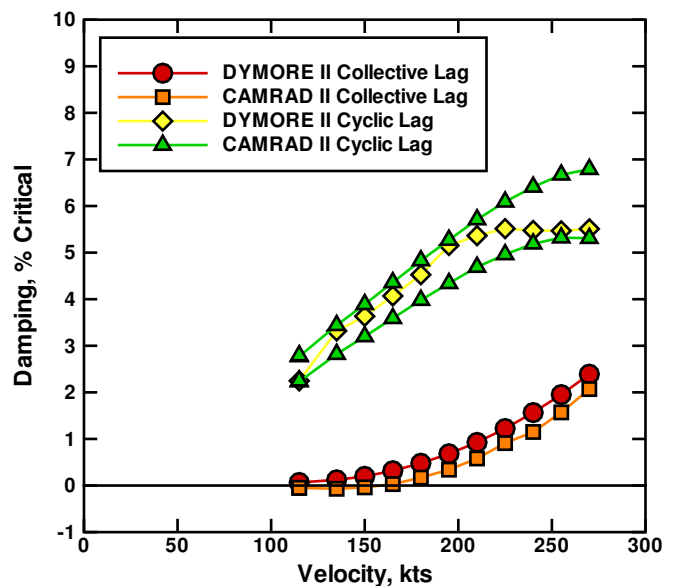


Fig. 15. Comparison of isolated rotor lag damping from CAMRAD II and DYMORE II calculations, airplane mode, 1284 RPM.

Rotor-Wing Stability

The stability of the rotor and wing was assessed using DYMORE semi-span and full-span models. The information gained from the semi-span model should be equivalent to the symmetric modes of the full-span model. Anti-symmetric modes have different frequencies which depend on the mass properties of the fuselage.

A parametric study was conducted where a number of design parameters for both the rotor system and the wing were varied in order to determine their influence on wing beam mode damping. Stability was evaluated over the speed range of 75 kts to 330 kts. This range includes the entire operating envelope plus a margin of safety. Transition to helicopter mode should occur at the 1605 RPM, so 75 knots is well below the lowest airspeed where the vehicle should be operating at 1284 RPM.

If an instability occurs, motion should either grow without bound or reach a limit cycle, presumably with large amplitude. For the current configuration, no instabilities were found for the cases examined. Because the equations of motion are time integrated in DYMORE II, any instability in the system should be revealed, even if the unstable mode is not directly perturbed.

While the damping of every mode was not specifically tested, the absence of any unbounded response is an implicit indication that the rotor and wing model is stable. However, such a conclusion is not guaranteed, because loading variations due to maneuvers, gusts, and turbulence that are always present in flight in real air are not present in analysis. Only small perturbations due to discretization or round-off error are present. The wing beam mode has been shown to be the most critical for whirl flutter stability (Refs. 8–15), so most of the rotor-wing damping results presented in this work are for beam mode damping.

Previous work on tilt rotor aeroelasticity also provides guidance for where to find the critical conditions. The critical flight condition for whirl flutter has been shown to be the windmilling condition. So many of the results presented here are for a windmilling rotor. To trim the rotor in a windmilling condition, the airspeed and rotor speed were set and the collective pitch was adjusted to obtain zero torque on the drive shaft.

Wing aerodynamics were not included in the semi-span parametric study. Beam mode damping due to wing aerodynamics is a function of airspeed only and can be separated from dynamics of the rotor system. The purpose of the current work is to assess the stability of a proposed rotor and wing design, so it was beneficial to remove the offset provided by wing aerodynamics to obtain a clearer picture of the parametric effects.

To illustrate, Figure 16 shows the beam mode damping at the airplane mode and helicopter mode rotor speeds both with

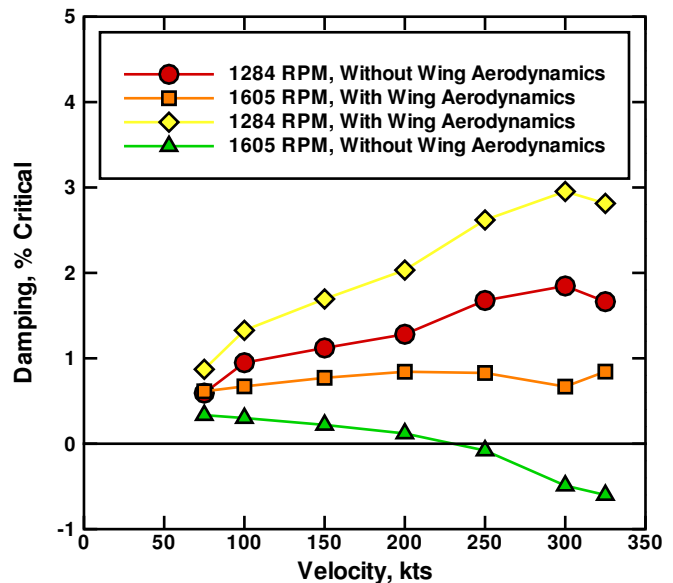


Fig. 16. Comparison of beam mode damping in airplane mode 1284 RPM and 1605 RPM with and without the effects of wing aerodynamics.

and without wing aerodynamics. The wing aerodynamics add an increment to the beam mode damping that is linear with airspeed. To more clearly see the linearity, the data with and without wing aerodynamics were subtracted for each airspeed to obtain the plot shown in Figure 17. A dashed line from the origin to the first data point was added to show that the lines do intersect the origin. With the exception of the highest airspeed, the damping increment is linear with velocity, but independent of rotor speed. The wing aerodynamics can be added by superposition to the parametric results. The baseline for the parametric study is the red line with circular symbols in Figure 16.

DYMORE does not use modal reduction, so modal structural damping cannot be added directly to the model. Damping must be added as part of the distributed properties and its effect on damping of modes is not intuitive. Therefore, structural damping was set to zero for the stability calculations. Any assumed structural damping can be added by superposition.

The first parameter to be varied was the lagwise bending stiffness of the rotor blades. Note that the stiffness changes indicated are only for the blade flexure (see Figure 2), not the entire blade. Changing the flexure stiffness changes the first elastic chordwise mode, but has a comparatively minor effect on higher modes. It also restricts the change to inplane motion, that is, in the hub coordinate system, whereas changes to the entire blade would shift frequencies differently depending on collective pitch.

The result is shown in Figure 18. The beam mode stability is largely insensitive to lag stiffness. A large excursion in lag

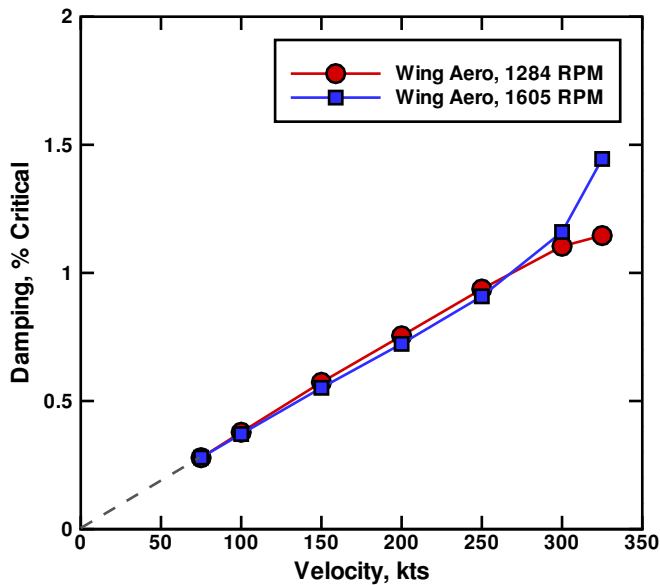


Fig. 17. Beam mode damping from wing aerodynamics in airplane mode.

stiffness, where the stiffness is only 25% of the baseline, only produces a small change in damping. Halving the stiffness, which could arguably also be called a large excursion, has only a minor effect on damping. Increasing the lag stiffness does not produce any significant increase in stability.

The second parameter was non-structural tip weight. The baseline configuration has some tip weight included in the running mass. For the parametric study, the tip weight was increased in addition to the baseline value. Additional tip weight has the combined effect of increasing the rotor mass and inertia, and reducing its Lock number. The results are shown in Figure 19. The tip weights uniformly destabilize the rotor at low speed, but stabilize it at high speed. The 1.5 lb and 2.0 lb damping lines are nearly identical, suggesting that larger tip weights would have little effect.

A parameter that had a sizable impact on damping was the blade precone angle. The baseline precone was 2 deg. Variations from 0 to 4 deg are shown in Figure 20. There is little effect below 200 kts, but at high speed, the beam damping varies significantly. At the maximum speed of 330 kts it ranges from less than 0.5% critical with 4 deg precone to nearly 3.5% with no precone. The fan-like distribution of damping where the spreading of points increases with airspeed suggests that aerodynamic effects play the dominant role relative to inertial effects of changing the blade geometry.

The first fixed-system parameter to be changed was the beamwise bending stiffness. Unlike the blade lag stiffness, the beamwise bending stiffness was modified by scaling the bending stiffness along the entire wing span. The effects of increasing and decreasing stiffness are shown in Figure 21. The effects are greatest at low speed, where the influence of

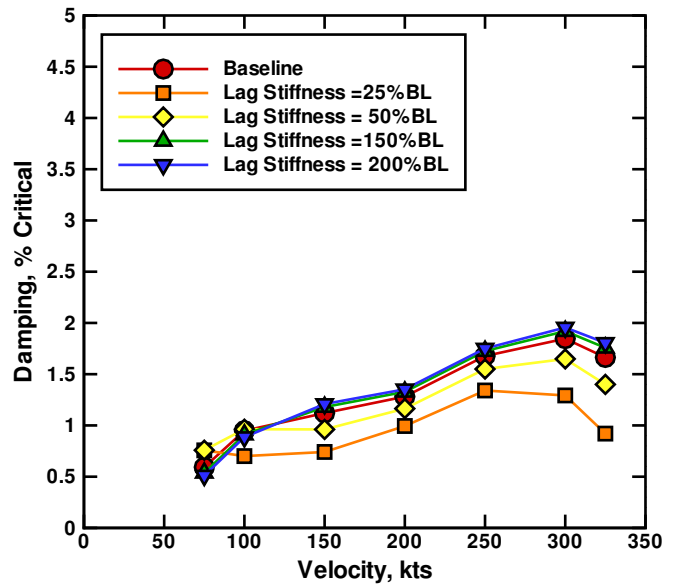


Fig. 18. Variation of wing beam damping with blade lag-wise bending stiffness, airplane mode, 1284 RPM.

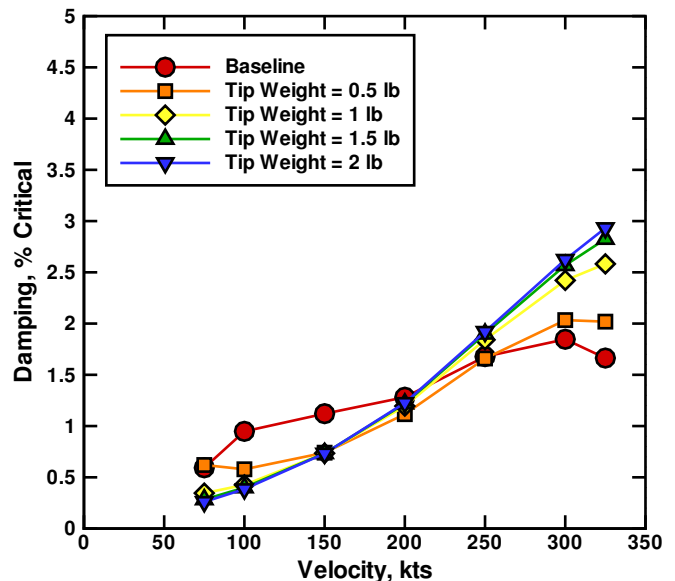


Fig. 19. Influence of added blade tip weight on wing beam damping, airplane mode, 1284 RPM.

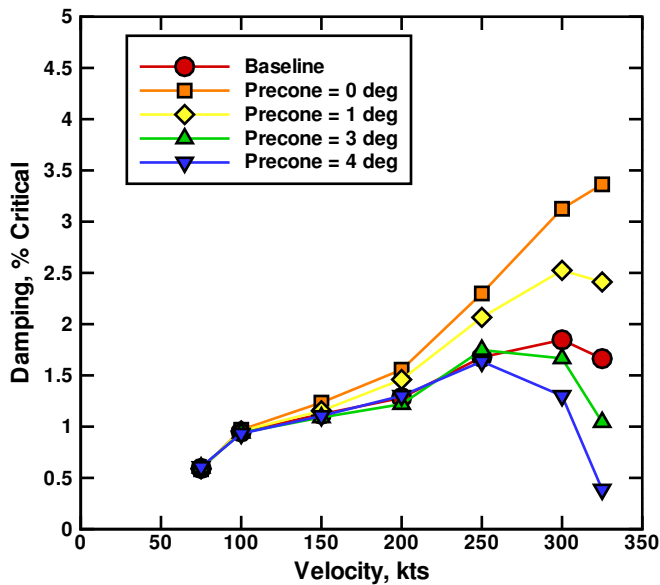


Fig. 20. Variation of wing beam damping with blade precone, airplane mode, 1284 RPM.

aerodynamics is smaller. As stated above, below 150 kts, the aircraft should be in conversion to helicopter mode, so for practical purposes, this region is not of interest. At high and low speed, the trend is for increasing damping with increasing stiffness. At 200 kts, the half stiffness damping is higher than the baseline, but is approximately the same or lower for the other data points. A single outlying point is probably caused by numerical error rather than a physical phenomenon.

The variation in damping with the wing chordwise stiffness is shown in Figure 22. There is virtually no sensitivity to chordwise stiffness evident over the entire speed range. Even a 50% increase or decrease in stiffness does not produce a noticeable change in damping over the entire speed range. Chordwise wing bending produces axial motion of the hub. It is largely decoupled from inplane hub motion, at least in the first chordwise mode. The collective blade flapping produced by axial hub motion is heavily damped, so there is little effect on rotor-wing stability.

The effect of wing torsion stiffness is shown in Figure 23. Unlike chordwise bending stiffness, torsion stiffness has a measurable effect on beam damping at high speed. Because of the chordwise offset of the hub with respect to the wing, torsion produces pylon pitch motion and inplane (that is, in the rotor plane) motion of the hub. The inplane hub motion couples with the blade lag mode and affects the stability of the rotor-wing system. Like rotor precone, there is little effect below 200 kts. Above 200 kts, reductions in torsion stiffness reduce the beamwise damping. The reduction is modest for a 25% reduction in stiffness, more noticeable for a 50% reduction. Increasing the stiffness above the baseline produces only a modest increase.

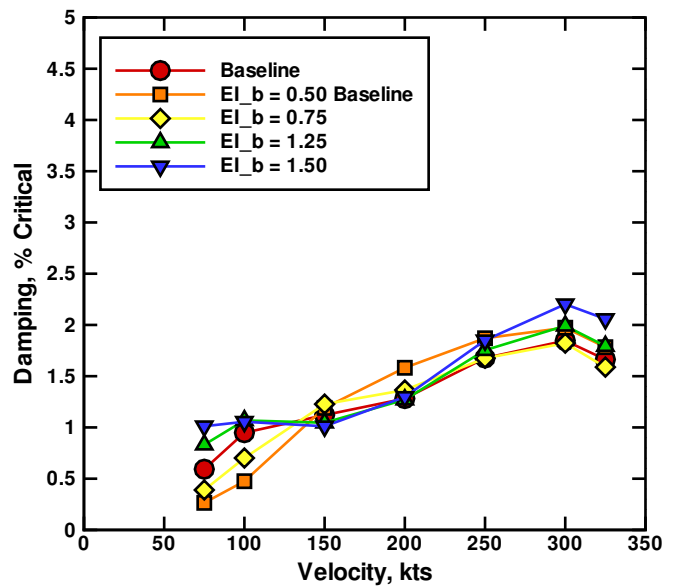


Fig. 21. Variation of wing beam damping with wing beamwise bending stiffness, airplane mode, 1284 RPM.

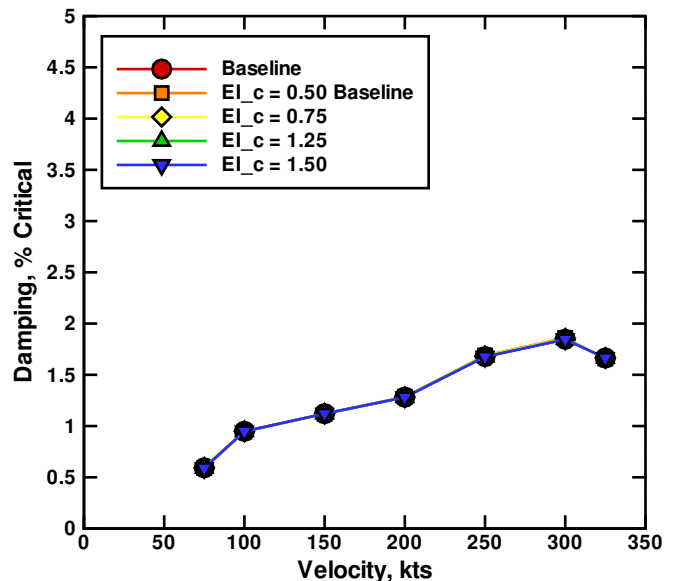


Fig. 22. Variation of wing beam damping with wing chordwise bending stiffness, airplane mode, 1284 RPM.

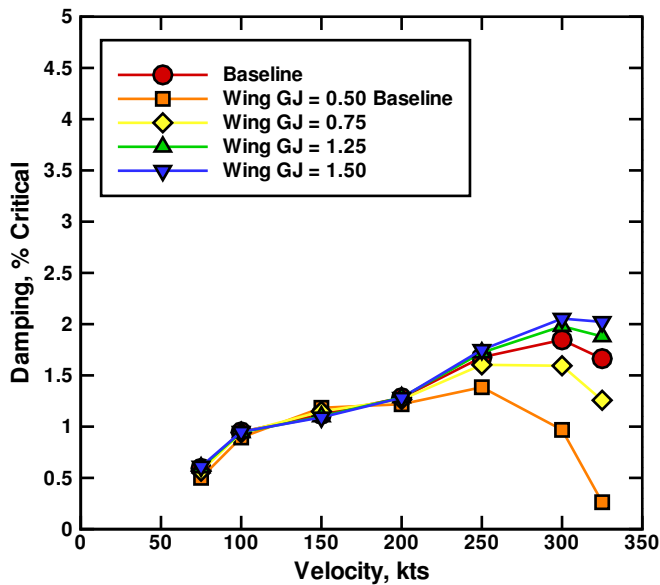


Fig. 23. Variation of wing beam damping with wing torsion stiffness, airplane mode, 1284 RPM.

Pylon pitch motion is a combination of wing elastic torsion and compliance in the conversion spring. As the wing torsion stiffness increased, it eventually becomes rigid relative to the conversion spring and vice versa. Then the compliant part produces all of the motion and increases in the stiffness of the rigid part do not increase damping.

The effect of the pylon spring is shown in Figure 24. Like wing torsion stiffness, it has a noticeable effect on rotor-wing damping. For increases in conversion stiffness, the damping asymptotically approaches a maximum value around 2.5% critical. By lowering the conversion spring stiffness, damping is reduced, particularly at high speed. For the half stiffness case, neutral stability is observed at 300 kts. Even at low speed, a small decrease in damping is predicted.

The last parameter to be examined with the semi-span model was mast height. Changing the length of the mast alters the separation of the hub from the wing bending and torsion axes. This has the effect of increasing the hub motion due to wing torsion, but also increasing the torsional inertia of the rotor-wing system. The mast height was only changed over a small $\pm 10\%$ range. The increments shown are percentages of the distance from the wing quarter chord to the hub, not the length of a specific piece of hardware. The distance would include both pylon and rotor components on the real airframe. As shown in Figure 25, there is little change in damping with this small variation. The influence does seem to increase at high speed, although the spread of damping at 150 kts is nearly as large as that at 300 kts. For practical purposes, the damping is insensitive to the small variations in mast height.

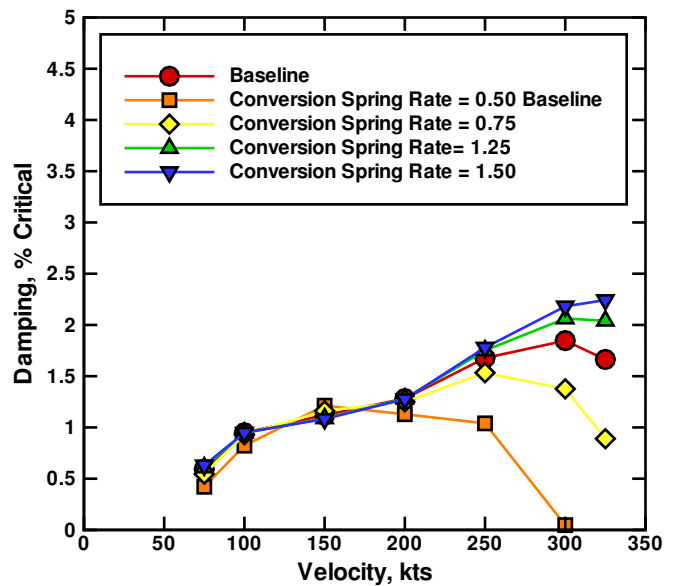


Fig. 24. Variation of wing beam damping with pylon conversion spring stiffness, airplane mode, 1284 RPM.

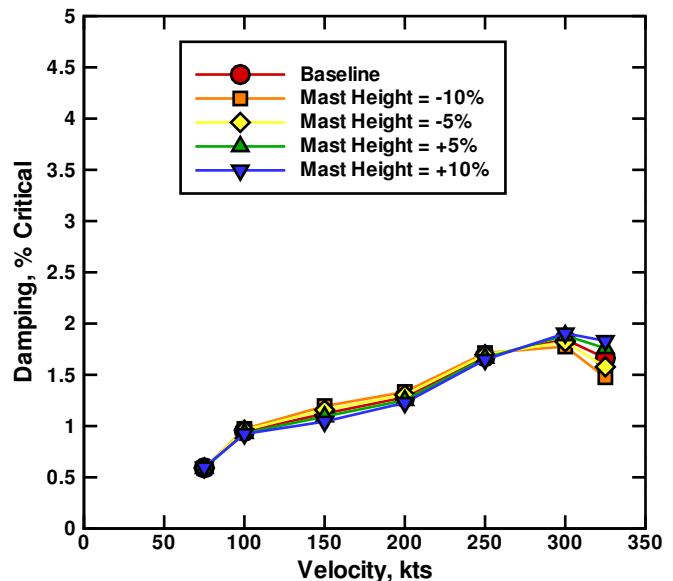


Fig. 25. Variation of wing beam damping with blade rotor mast height, airplane mode, 1284 RPM.

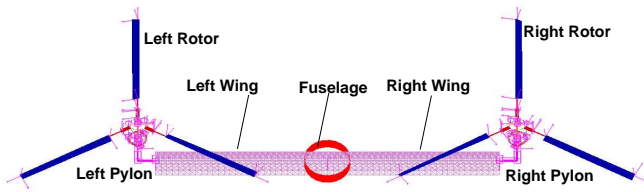


Fig. 26. DYMORE II full-span rotor and wing model.

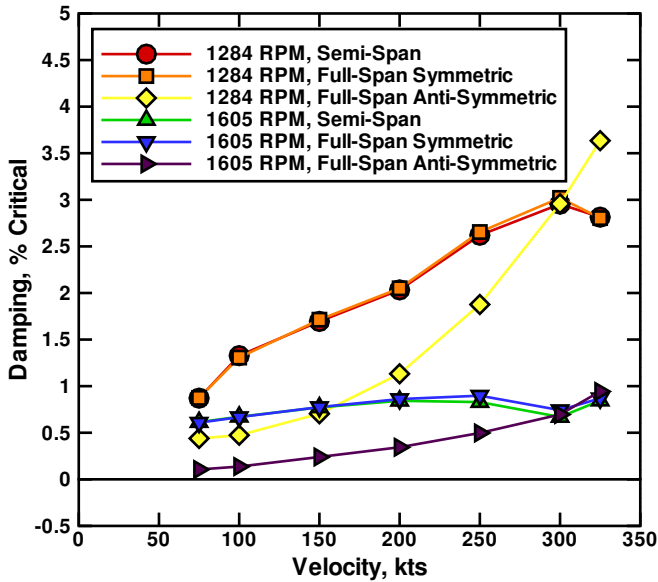


Fig. 27. Comparison of damping ratios of semi-span and full-span beamwise bending modes with wing aerodynamics at 1284 RPM and 1605 RPM.

Full-Span Model

A full-span model was also developed in DYMORE II to examine the stability of both symmetric and anti-symmetric wing modes. The symmetric wing modes should be identical to the semi-span modes, while the anti-symmetric modes are different in both frequency and damping. There is a rigid body roll mode that produces anti-symmetric wing deflection, but this mode has no elastic energy and is not of interest in the current study. The first elastic anti-symmetric mode is the mode of interest. The full-span model is shown in Figure 26.

For the full-span model, wing aerodynamics were included in the stability calculations. A comparison is shown in Figure 27. It is clear that for both 1605 and 1284 RPM, the semi-span and full-span symmetric modes are identical. The anti-symmetric modes have generally lower damping, but the damping monotonically increases with airspeed.

The only parametric variation considered with the full-span model was that of fuselage roll inertia. Variations in roll inertia are often found when fuel stored in the wings is burned

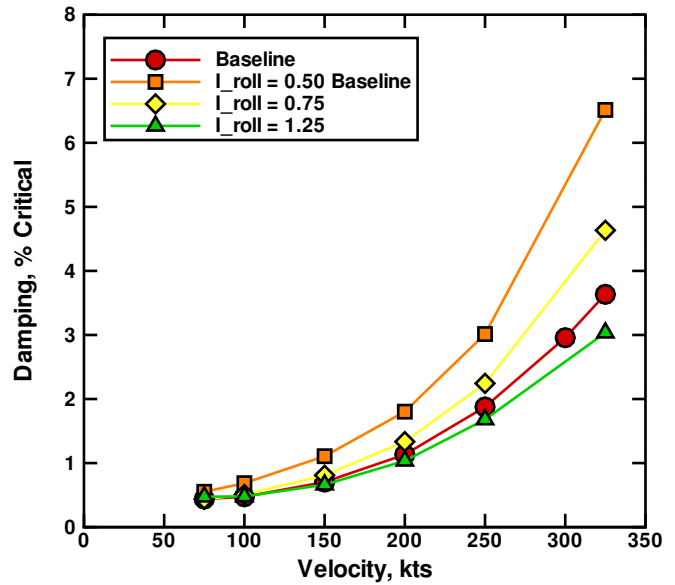


Fig. 28. Variation of damping in the anti-symmetric wing beam mode with fuselage roll inertia, airplane mode, 1284 RPM.

off, and to a lesser extent by changes in payload in the main fuselage. To simulate these changes, the roll inertia was varied from one half to 125% of the baseline inertia. Figure 28 shows that reducing the roll inertia due to fuel burn improves the stability, significantly at high speed. An increase in inertia has a detrimental effect, but it is minor for a 25% increase. Unlike decreasing inertia from fuel burn, an increase above the full-fuel gross weight would likely be a payload modification near the vehicle cg. The small moment arm implies an equivalent increase in gross weight, where 25% would be substantial without further modifications to the rotors and/or engine.

Conclusions

Loads and stability calculations using the comprehensive analysis CAMRAD II and the multibody dynamics analysis DYMORE II have been presented, including comparisons of calculations between the two analyses. Based on the results of the current study, the following conclusions are offered.

1. Correlation of flap and lag bending moments between CAMRAD II and DYMORE II was good particularly in airplane mode.
2. Torsion moments did not compare well between the two analyses, with differences ranging from 50% to 200%.
3. Isolated rotor lag damping calculations were almost exactly the same between the two analyses despite different methods of calculating damping.

4. A parametric study of wing beam mode damping revealed no instabilities over a broad speed range.
5. Beam mode damping was found to be particularly sensitive to blade precone angle, wing torsion stiffness, and pylon conversion actuator stiffness. Reduced fuselage roll inertia due to fuel burn was found to increase beam mode damping.

References

- ¹Johnson, W., "Technology Drivers in the Development of CAMRAD II," Proceedings of the American Helicopter Society Aeromechanics Specialists Conference, San Francisco, CA, January 1994.
- ²Bauchau, O. A., Bottasso, C., and Nikishkov, Y., "Modeling Rotorcraft Dynamics with Finite Element Multibody Procedures," *Mathematical and Computer Modeling*, Vol. 33, 2001.
- ³Shen, J., Singleton, J. D., Piatak, D. J., and Bauchau, O. A., "Multibody Dynamics Simulation and Experimental Investigation of a Model-Scale Tiltrotor," Proceedings of the American Helicopter Society 61st Annual Forum, Grapevine, TX, June 2005.
- ⁴Johnson, W., "Calculation of Tilt Rotor Aeroacoustic Model (TRAM DNW) Performance, Airloads, and Structural Loads," Proceedings of the American Helicopter Society Aeromechanics Specialists Conference, Atlanta, GA, November 2000.
- ⁵Shen, J., Floros, M. W., Lee, M. K., and Kim, J. M., "Multibody Dynamics Simulation of a Tiltrotor UAV," Proceedings of the Second International Basic Research Conference on Rotorcraft Technology, Nanjing, China, November 2005.
- ⁶Hwang, S., Lee, M. K., Kim, Y., and Kim, J. M., "Proprotor Load Evaluation in Collision Avoidance Maneuver of Tilt Rotor Unmanned Aerial Vehicle," Proceedings of the AHS International Vertical Lift Design Conference, San Francisco, CA, January 2006.
- ⁷Bauchau, O. A. and Wang, J., "Stability Analysis of Complex Multibody Systems," *Journal of Computational and Nonlinear Dynamics*, Vol. 1, (1), January 2006.
- ⁸Johnson, W., "Dynamics of Tilting Proprotor Aircraft in Cruise Flight," NASA TN D-7677, Ames Research Center, May 1974.
- ⁹Popelka, D. A., Sheffler, M., and Bilger, J., "Correlation of Test and Analysis for the 1/5th Scale V-22 Aeroelastic Model," *Journal of the American Helicopter Society*, Vol. 32, (2), April 1987.
- ¹⁰Settle, T. B. and Kidd, D. L., "Evolution and Test History of the V-22 0.2 Scale Aeroelastic Model," *Journal of the American Helicopter Society*, Vol. 37, (1), January 1992.
- ¹¹Nixon, M. W., "Parametric Studies for Tiltrotor Aeroelastic Stability in Highspeed Flight," *Journal of the American Helicopter Society*, Vol. 38, (4), October 1993.
- ¹²Idol, R. and Parham, T., "V-22 Aeroelastic Stability Analysis and Correlation With Test Data," Proceedings of the American Helicopter Society 51st Annual Forum, Fort Worth, TX, May 1995.
- ¹³Piatak, D. J., Kvaternik, R. G., Nixon, M. W., Langston, C. W., Singleton, J. D., Bennett, R. L., and Brown, R. K., "A Parametric Investigation of Whirl-Flutter Stability on the WRATS Tiltrotor Model," *Journal of the American Helicopter Society*, Vol. 47, (3), July 2002.
- ¹⁴Kvaternik, R. D., Piatak, D. J., Nixon, M. W., Langston, C. W., Singleton, J. D., Bennett, R. L., and Brown, R. K., "An Experimental Evaluation of Generalized Predictive Control for Tiltrotor Aeroelastic Stability Augmentation in Airplane Mode of Flight," *Journal of the American Helicopter Society*, Vol. 47, (3), July 2002.
- ¹⁵Nixon, M., Langston, C., Singleton, J. D., Piatak, D. J., Kvaternik, R., Corso, L. M., and Brown, R., "Aeroelastic Stability of a Four-Bladed Semi-Articulated Soft-Inplane Tiltrotor Model," Proceedings of the American Helicopter Society 59th Annual Forum, Phoenix, AZ, May 2003.